Supporting Information

Cation Exchange-Mediated Synthesis of Library of Plasmomagnetic Nanoheterostructures: Transformation of 2-Dimensional-Shaped Fe_7S_8 Nanoplates to Cu-Fe-S-Based Ternary Compound.

Dulal Barman†, Sirshendu Ghosh†, Sumana Paul, Biswajit Dalal and Subodh Kumar De*

Department of Materials Science, Indian Association for the Cultivation of Science, Jadavpur, Kolkata-700032, India

† Authors contributed equally

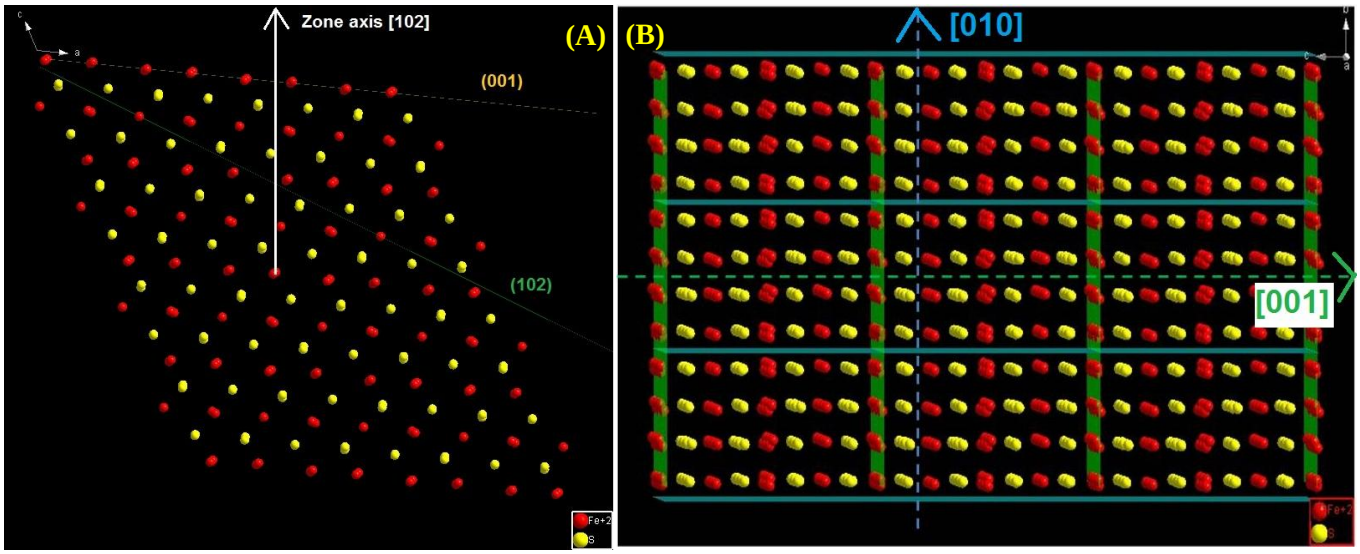

Figure S1. (A) shows the atomic model of (001) and (102) planes and zone axis [102] which indicates the most exposed facet or the upper surface of hexagonal nanoplate might be terminated with {001} facet. B) Atomic arrangement of Fe and S along [010] and [001] direction of Fe_7S_8 crystal.

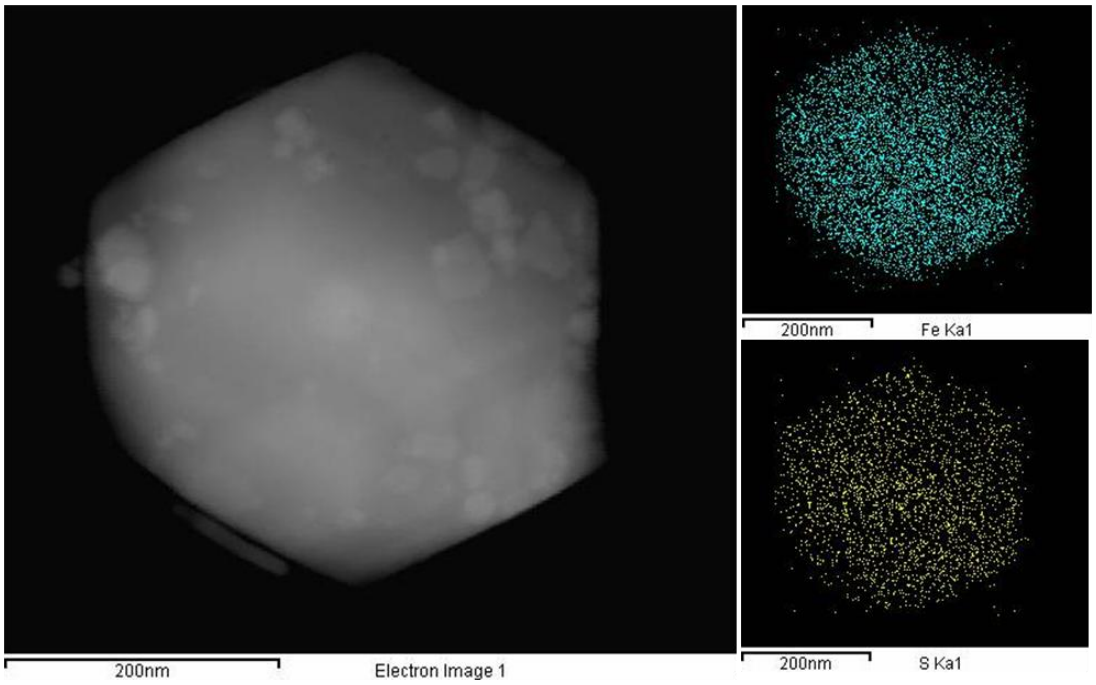

Figure S2. Elemental (Fe and S) mapping over a single Fe_7S_8nanoplate.

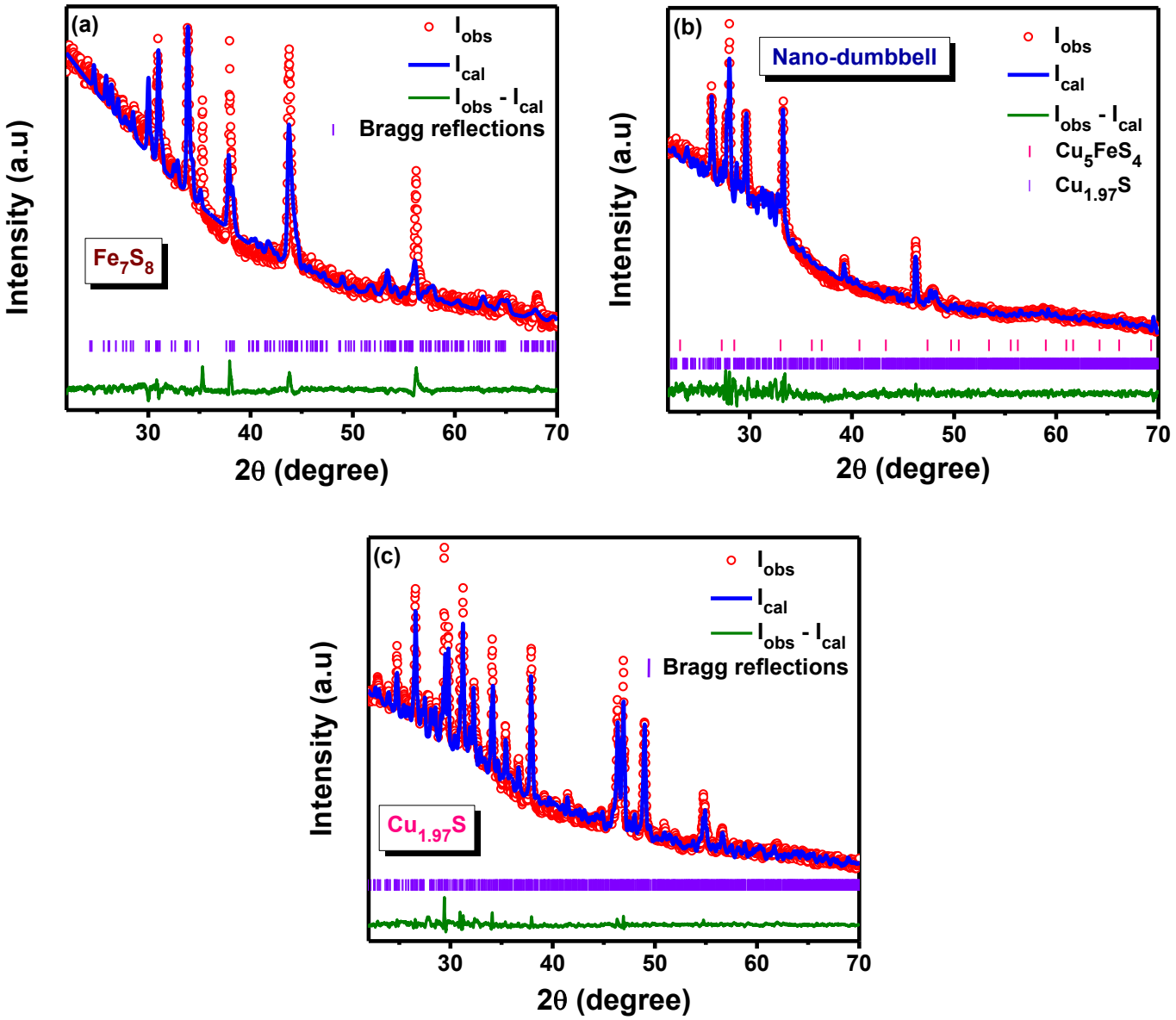

Figure S3. The room-temperature experimental x-ray diffraction data of pure Fe_7S_8, pure $Cu_{1.97}S$ and nanodumbbell (composite of Cu_5FeS_4 and $Cu_{1.97}S$ phases) samples are simulated with the help of Rietveld refinement of diffraction patterns using software MAUD[1]. The Cu_5FeS_4 and $Cu_{1.97}S$ phases have been fitted based on the observation of Ding et al. [2] and Howard T. Evans Jr. [3] respectively. The structural parameters obtained from the refinement are summarized in Table S 1. The obtained values of weighted profile factor (R_{wp} (in %)) for pure Fe_7S_8, pure $Cu_{1.97}S$ and nanodumbbell samples are 5.32, 8.34 and 4.11, respectively. The values less than 15 usually define an acceptable and good refinement for the complex phase like monoclinic.

Table S1: Refined lattice parameters along with the corresponding crystal structure and space group for pure Fe_7S_8, pure $Cu_{1.97}S$ and nanodumbbell samples.

Sample **Parameter**	**Fe_7S_8**	**$Cu_{1.97}S$**	**Nanodumbbell**	
			Phase-1 : $Cu_{1.97}S$	**Phase-2 : Cu_5FeS_4**
Structure	Monoclinic	Monoclinic	Monoclinic	Cubic
Space Group	*C2/c : b1*	*P21/c : a2*	*P21/c : a2*	*Fm-3m*
a (in Å)	11.894644	26.826721	27.021126	10.83514
b (in Å)	6.935642	15.686573	15.789024	10.83514
c (in Å)	12.992743	13.401268	13.619461	10.83514
angle (in degree)	$\beta = 117.9399$	$\alpha = 90.24138$	$\alpha = 90.29199$	$\alpha = \beta = \gamma = 90$

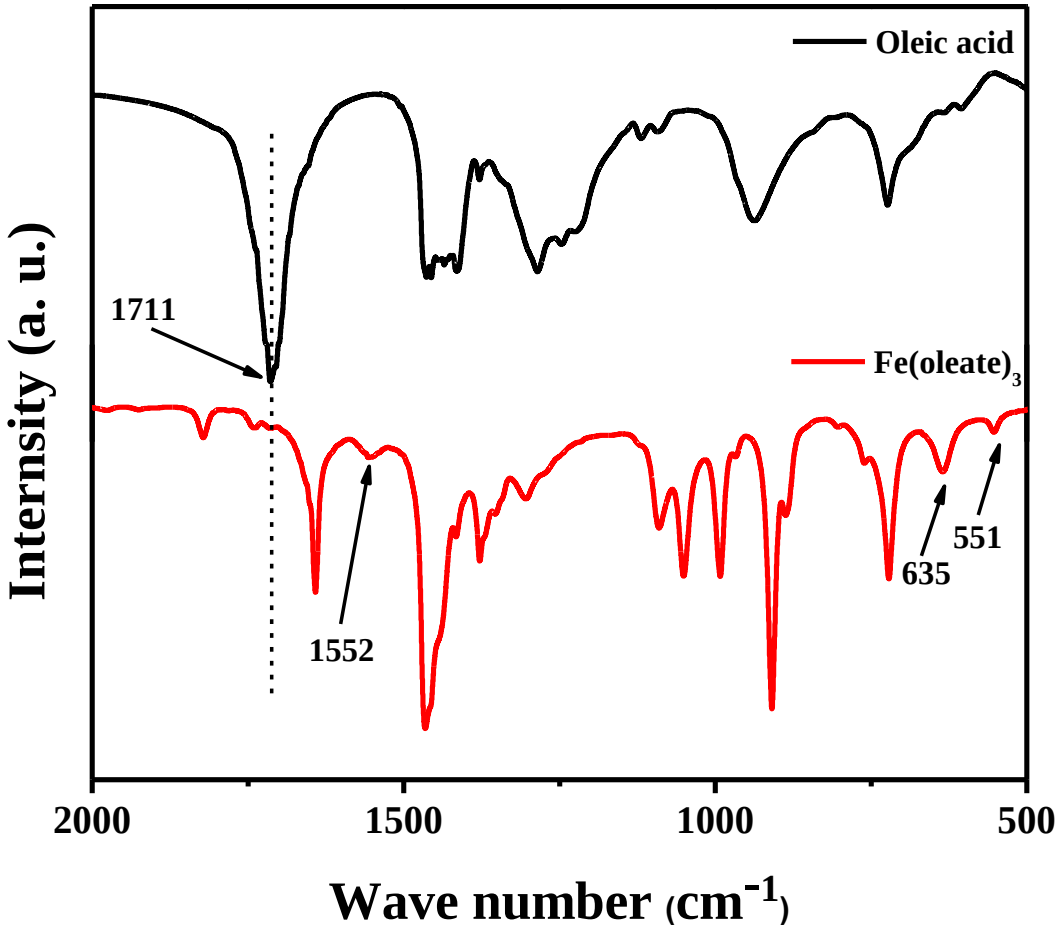

Figure S4. FTIR spectra of pure oleic acid and the washed liquid collected after centrifugation. The stretching frequency of Fe-oleate was appeared at 1552 cm^{-1} and Fe-O bond at 635 cm^{-1}.[4]

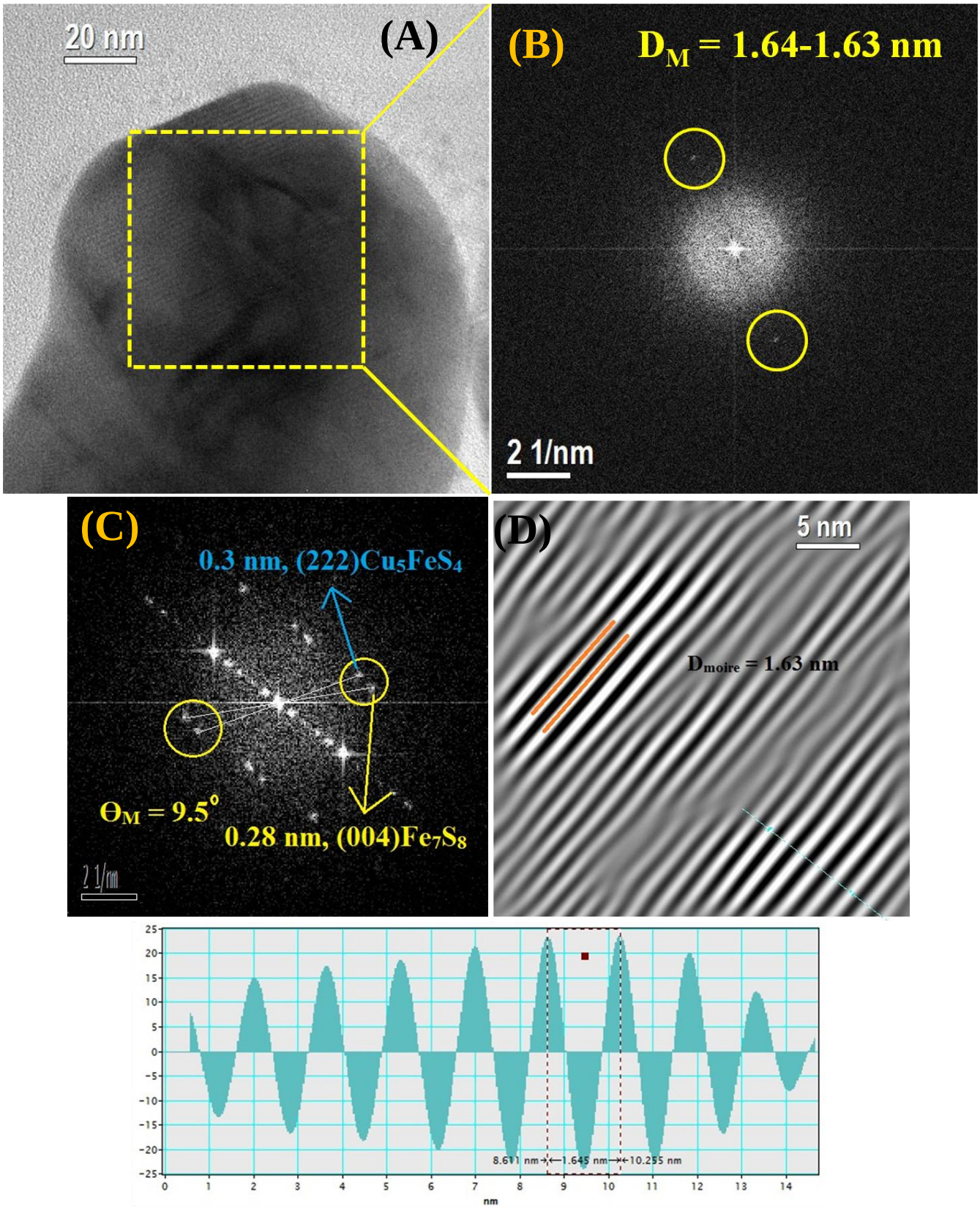

Figure S5. (A) TEM image shows the presence of Moiré pattern at the core-region. (B) FFT pattern of yellow square area shows a pair of well resolved spots corresponding to d_{Moire} value 1.63-1.64 nm.(C) Close interplanner distance of (222) plane of Cu_5FeS_4 and (004) of Fe_7S_8 makes an angle of ~ 9.5 °. (D) Simulated HRTEM of Moiré pattern.

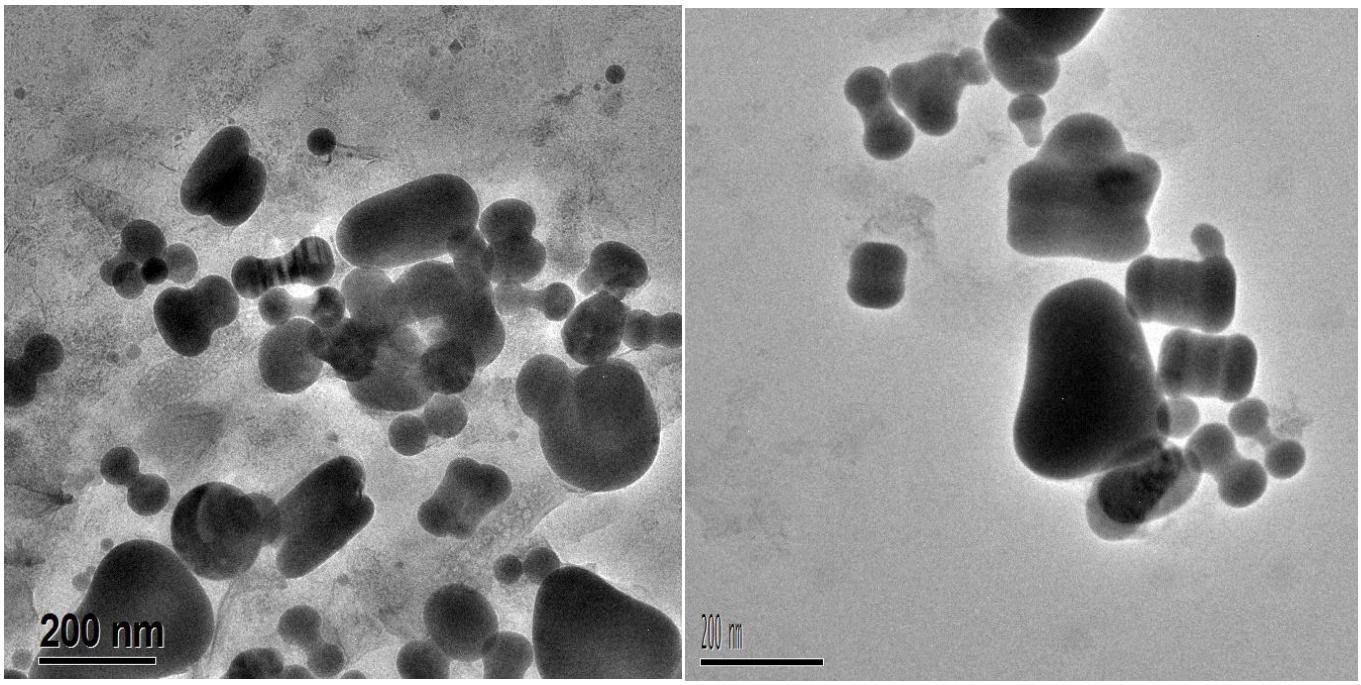

Figure S6. Large area TEM images of $Cu_{1.97}S/Cu_5FeS_4/Cu_{1.97}S$ nano dumbbells before size selective precipitation.

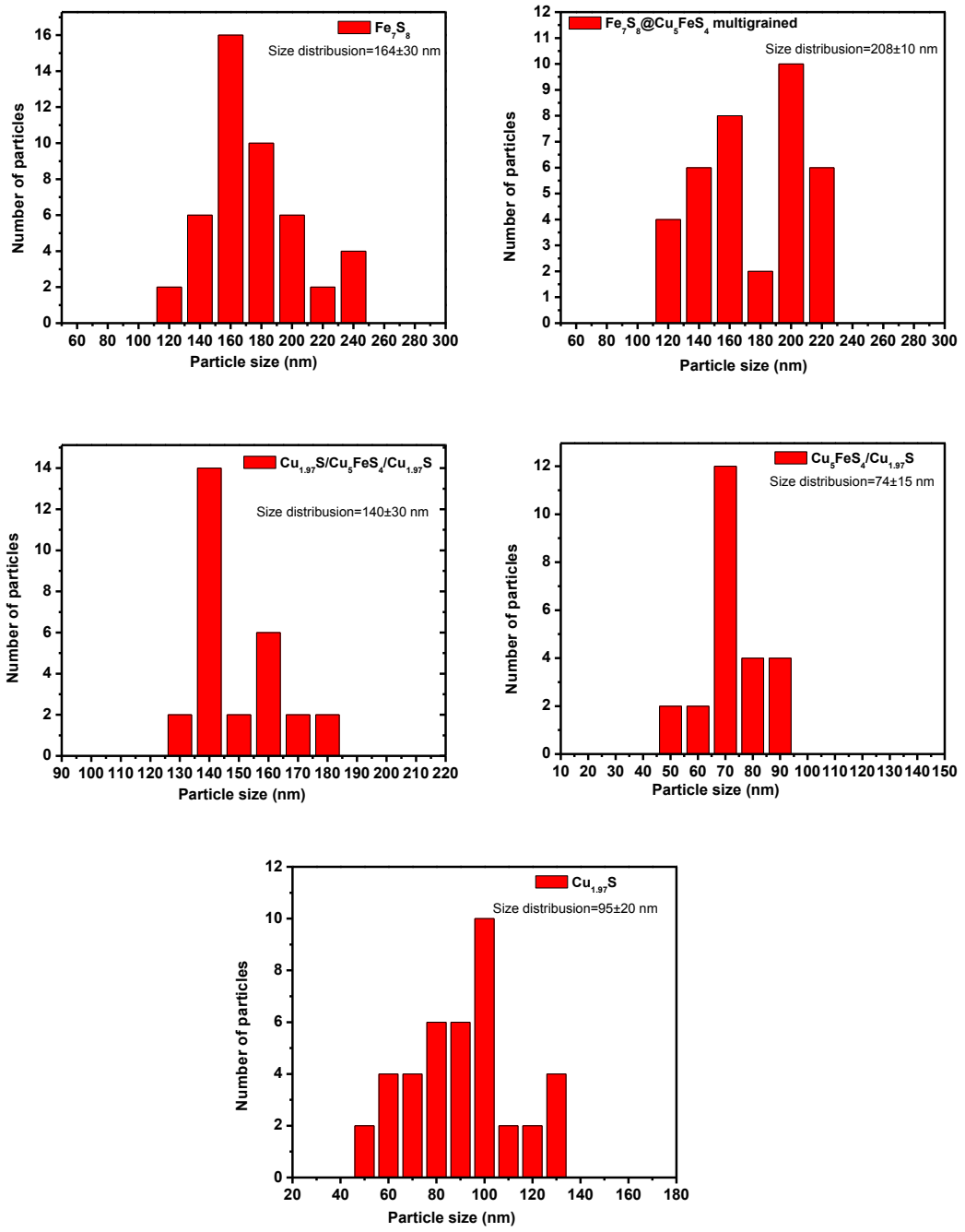

Figure S7. Histogram plots of different nanostructures.

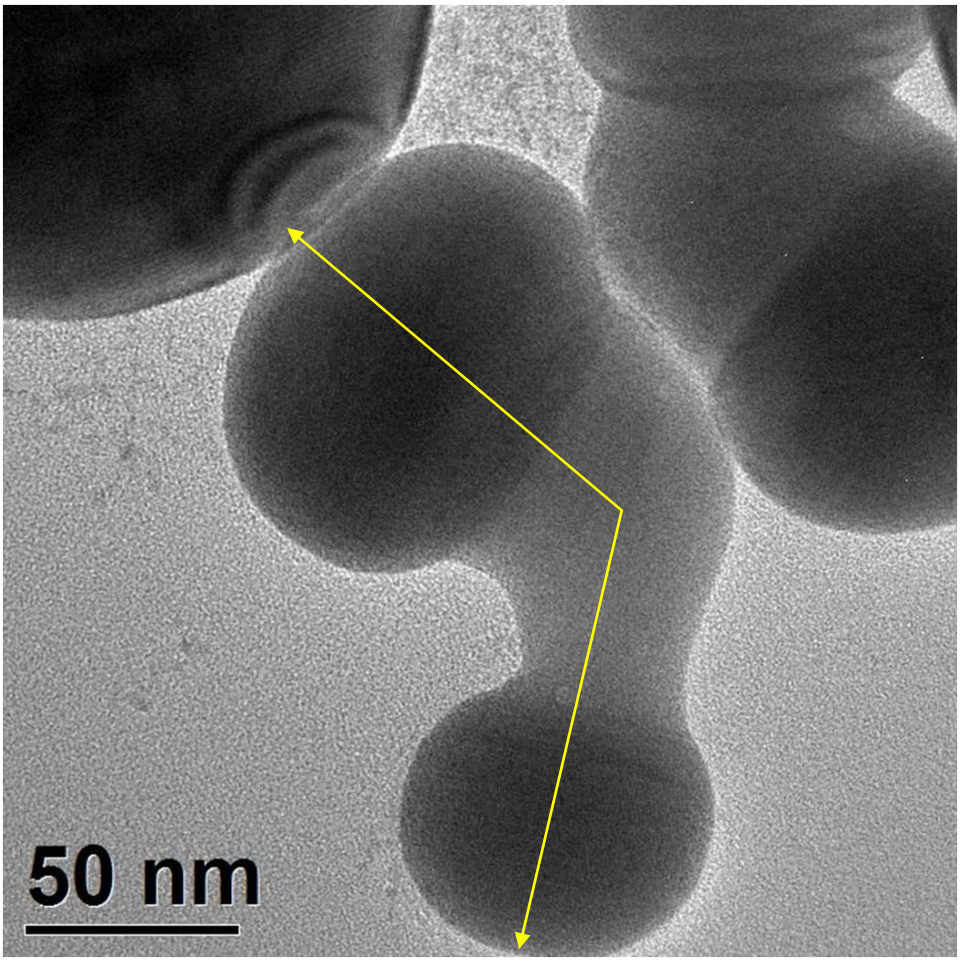

Figure S8. TEM image of two bent nanodumbell.

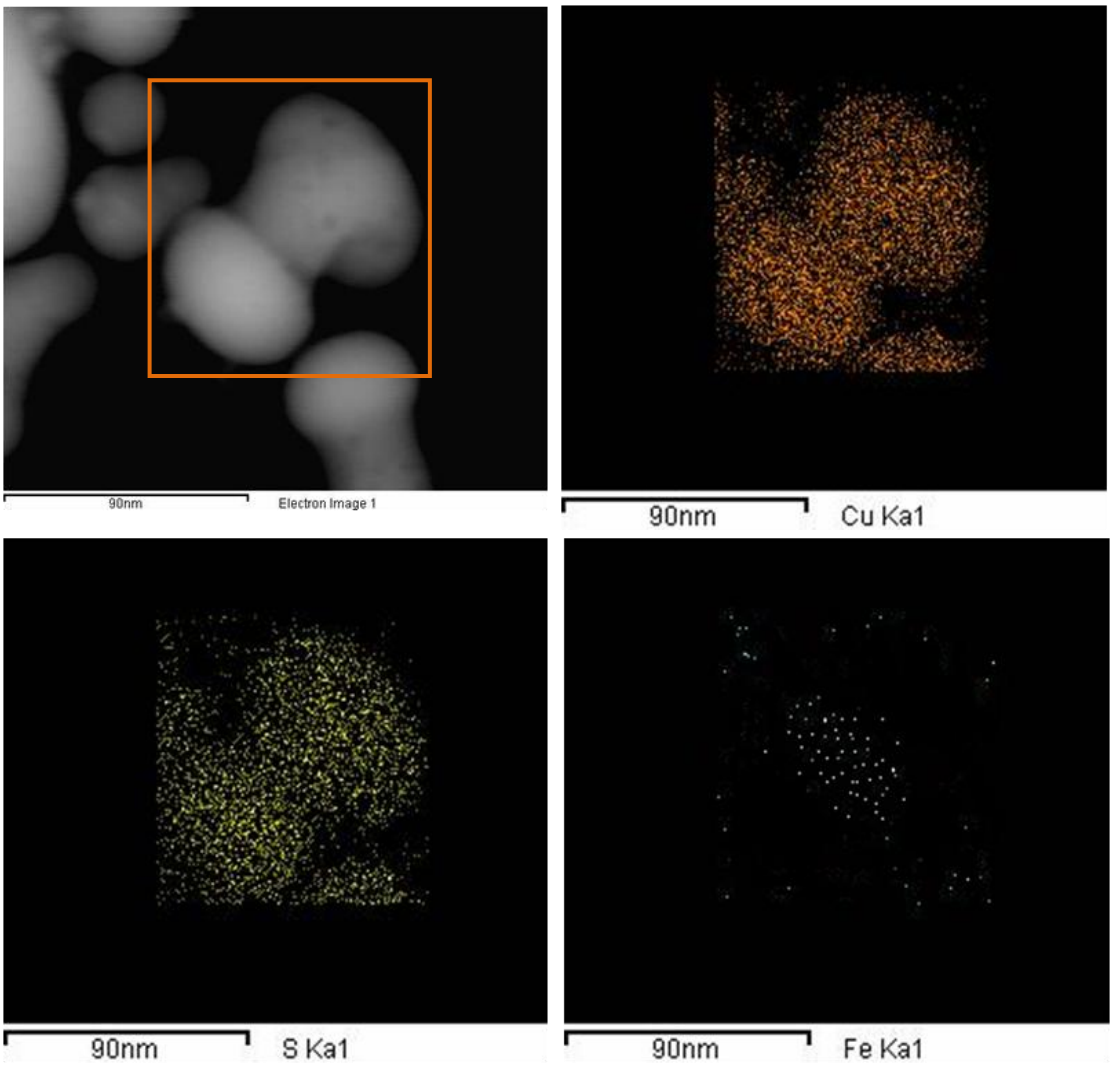

Figure S9. Element mapping over a single nanodumbell shows the presence of Cu and S throughout the nanocrystal and presence of Fe only at the middle part. Density of pixel for Cu at the hemisphere region is higher than the middle part.

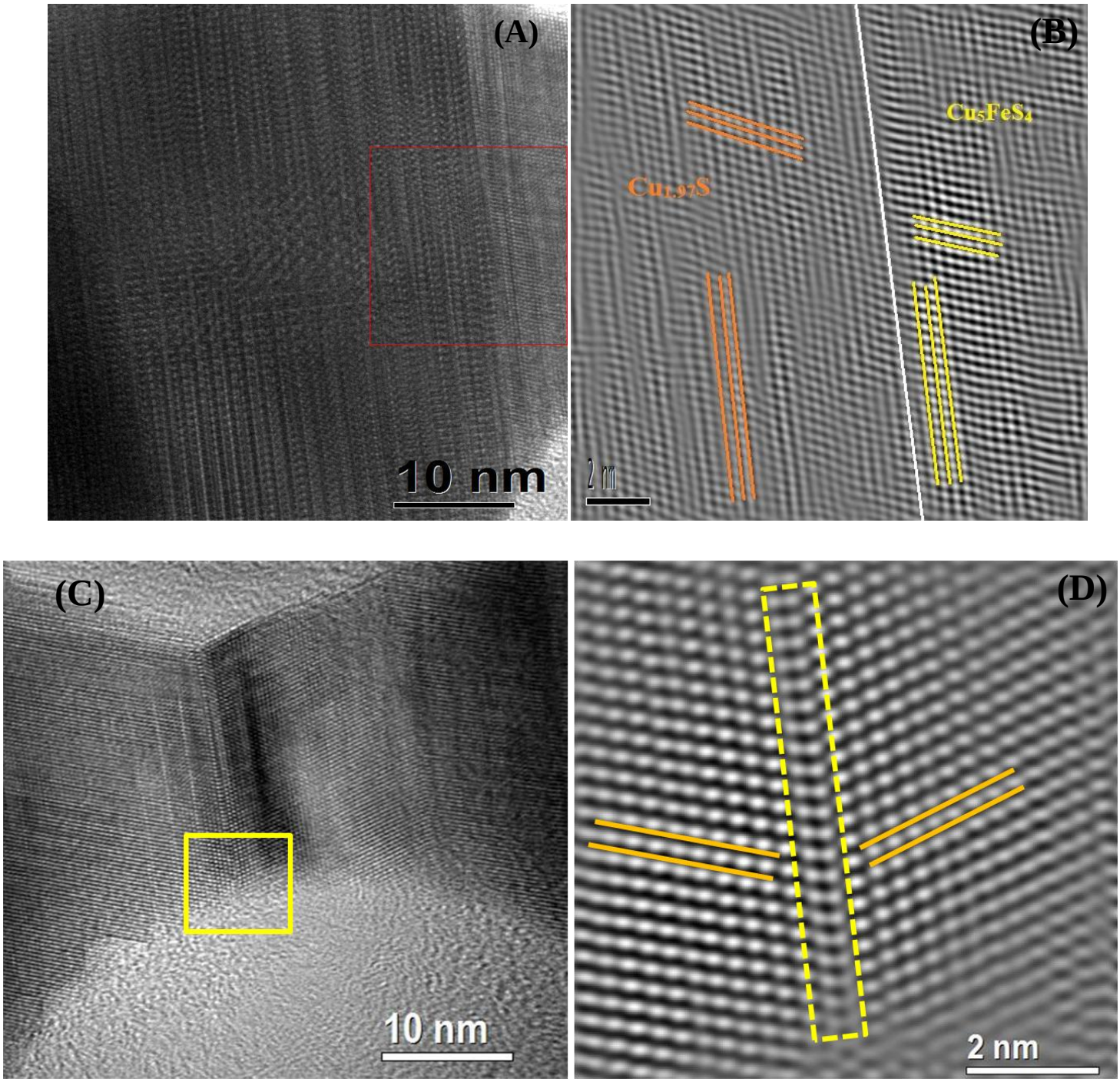

Figure S10. (A) and (B) TEM and reconstructed HRTEM of interface area of Cu1.97S and Cu5FeS4. (C) HRTEM image of middle part of nanodumbbell, (D) Reconstructed HRTEM image shows the grain boundary where two grain of Cu_5FeS_4 is connected by twin (1-13) planes at angle of 120 °.

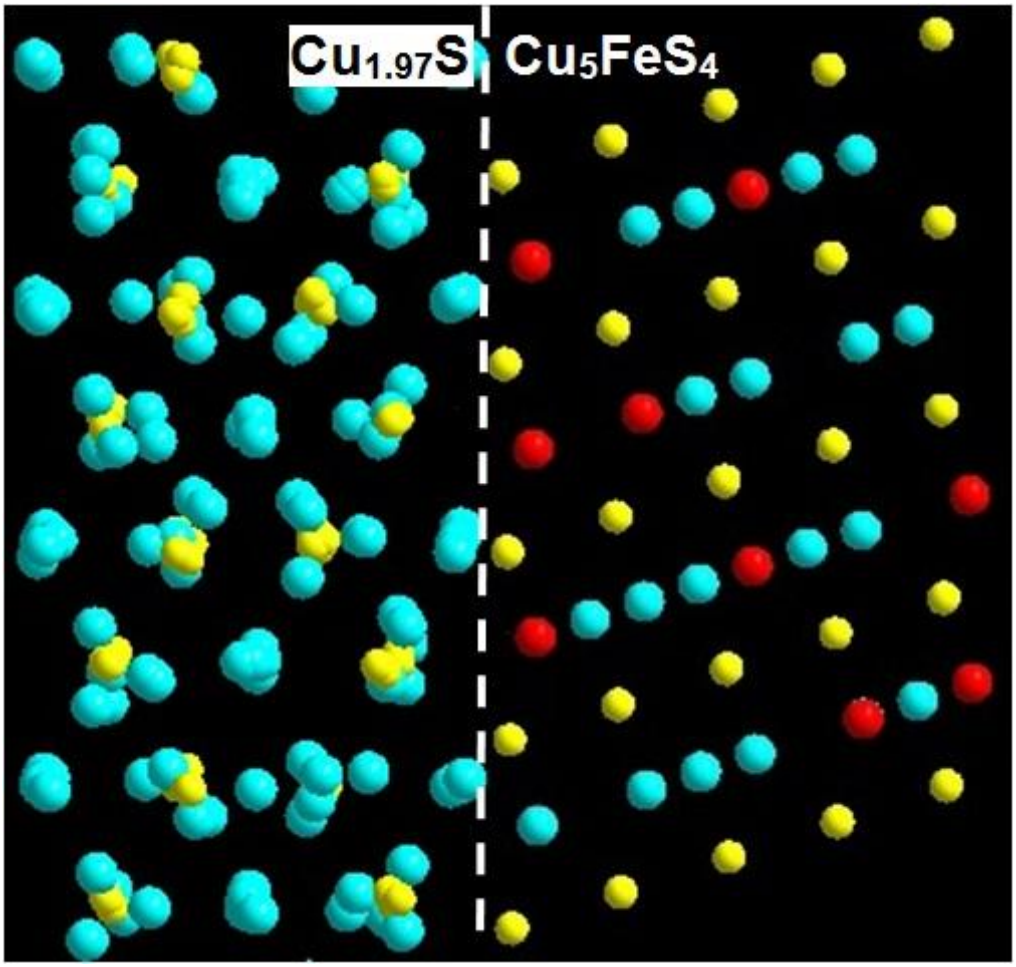

Figure S11. Atomic model of $Cu_{1.97}S$ and Cu_5FeS_4 along the epitaxy formation.

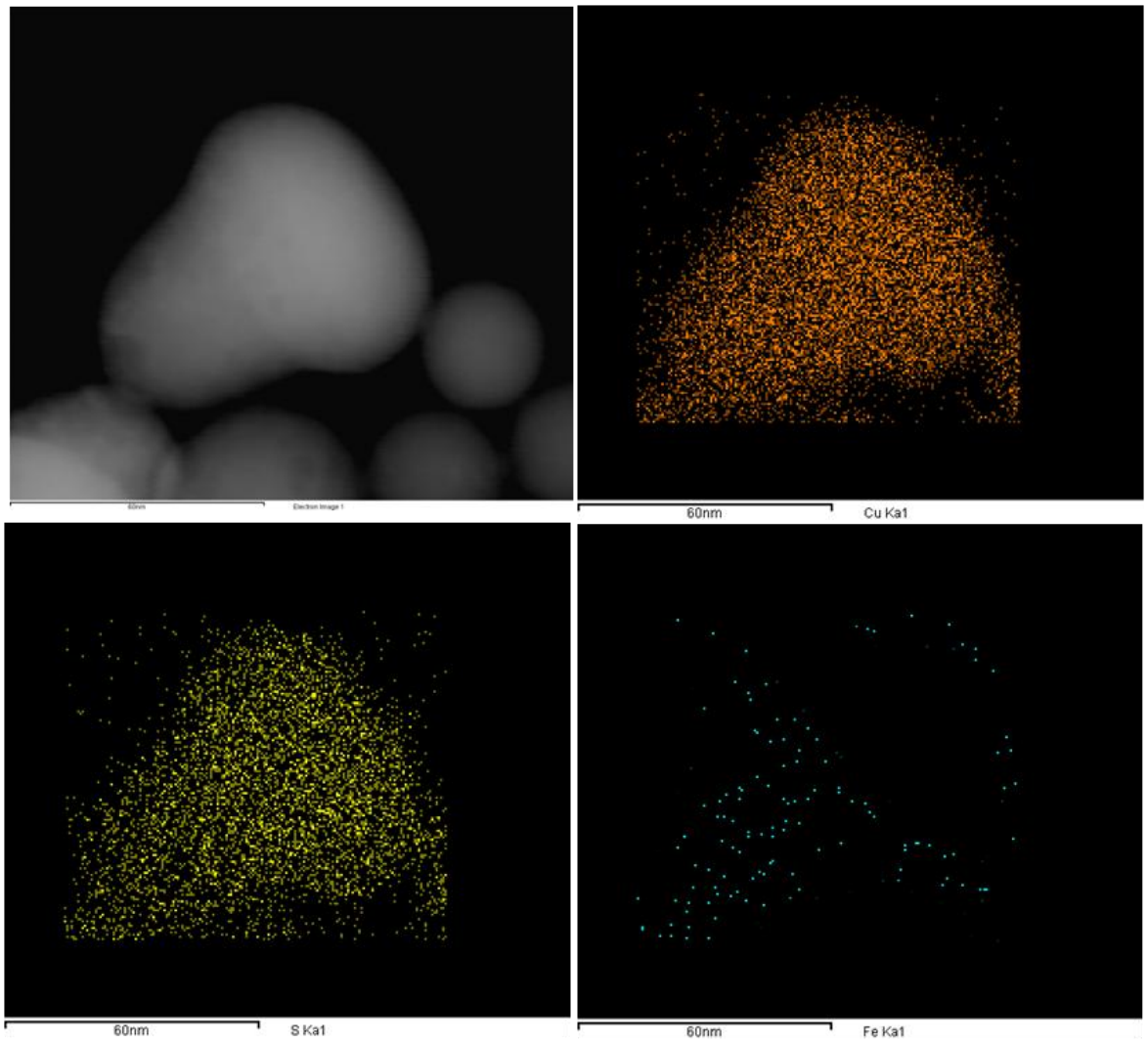

Figure S12. Element mapping over a single $Cu_5FeS_4/Cu_{1.97}S$ nanohat. Presence of Cu and S has been found throughout the structure whereas Fe only has been found only the top part.

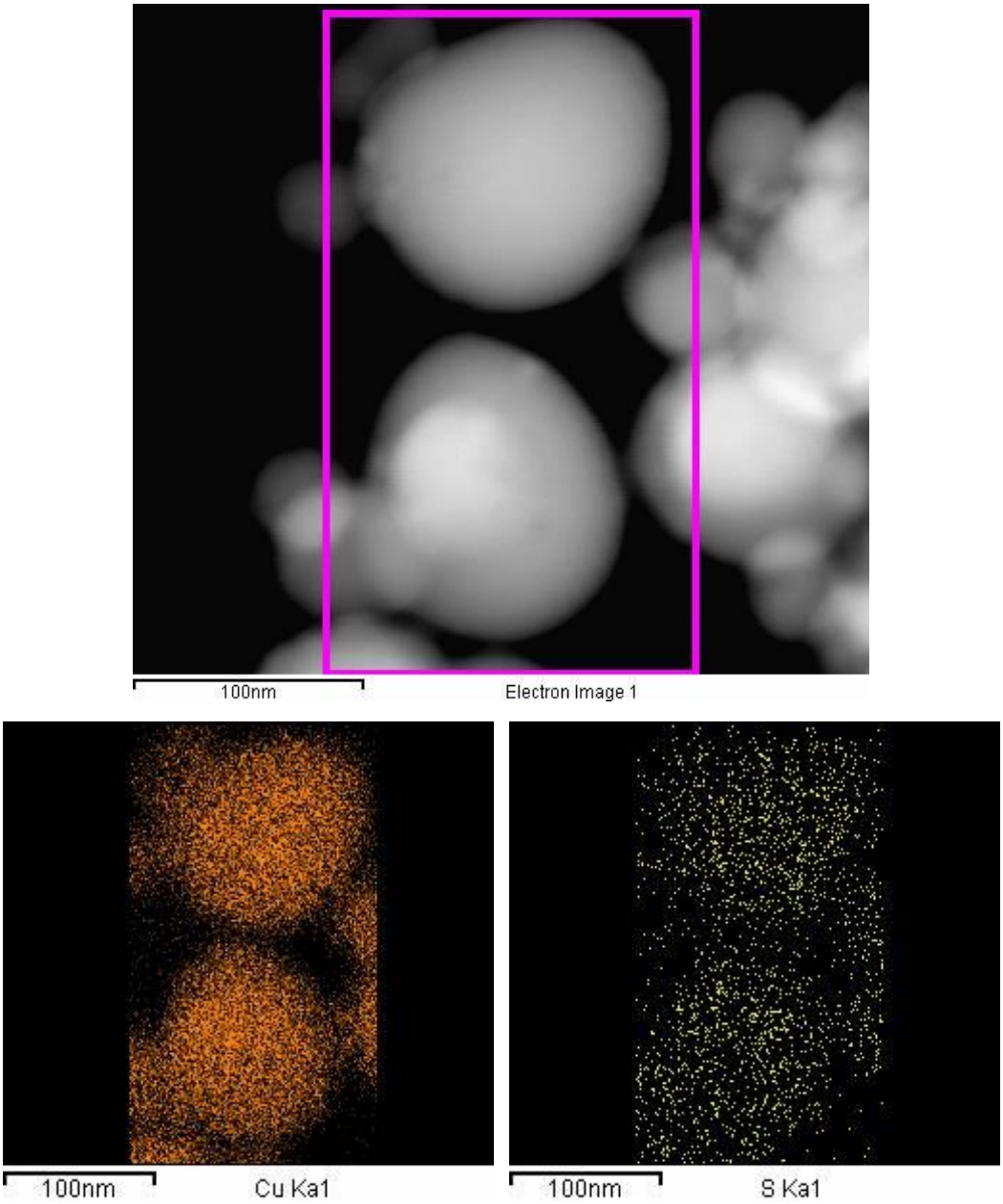

Figure S13. Element mapping over few $Cu_{1.97}S$ nanocrystals shows homogenous distribution of Cu and S.

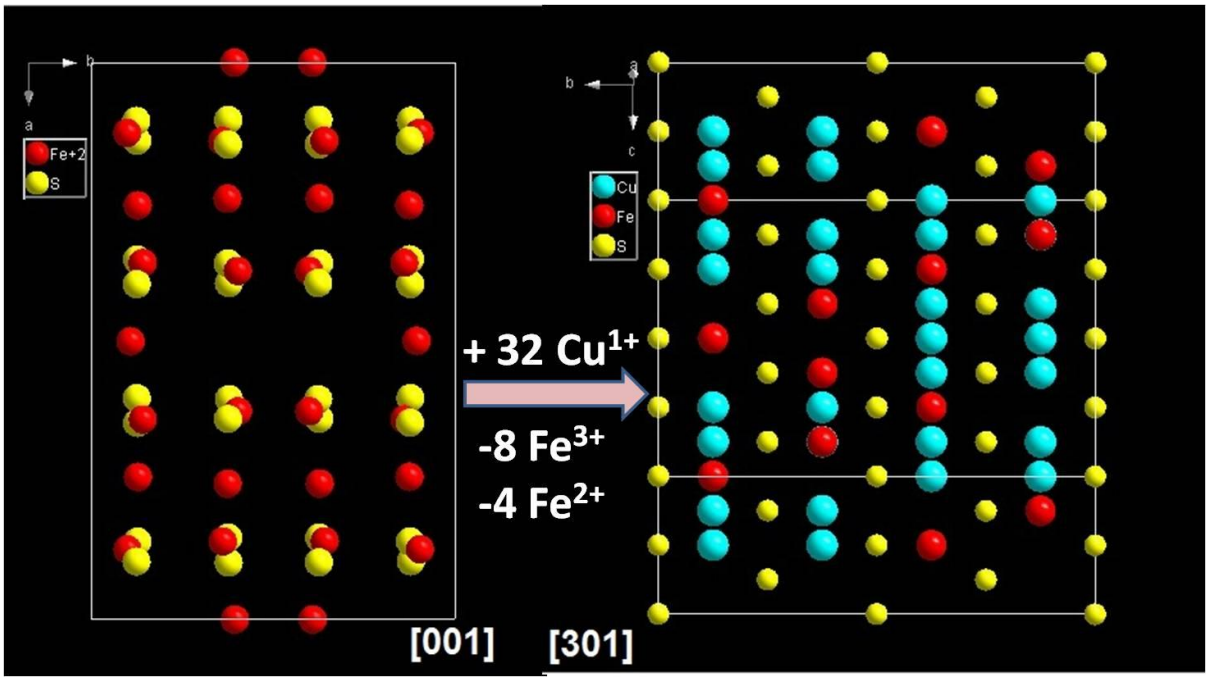

Figure S14. One unit cell of Fe_7S_8 and corresponding conversion of one unit cell of Cu_5FeS_4.

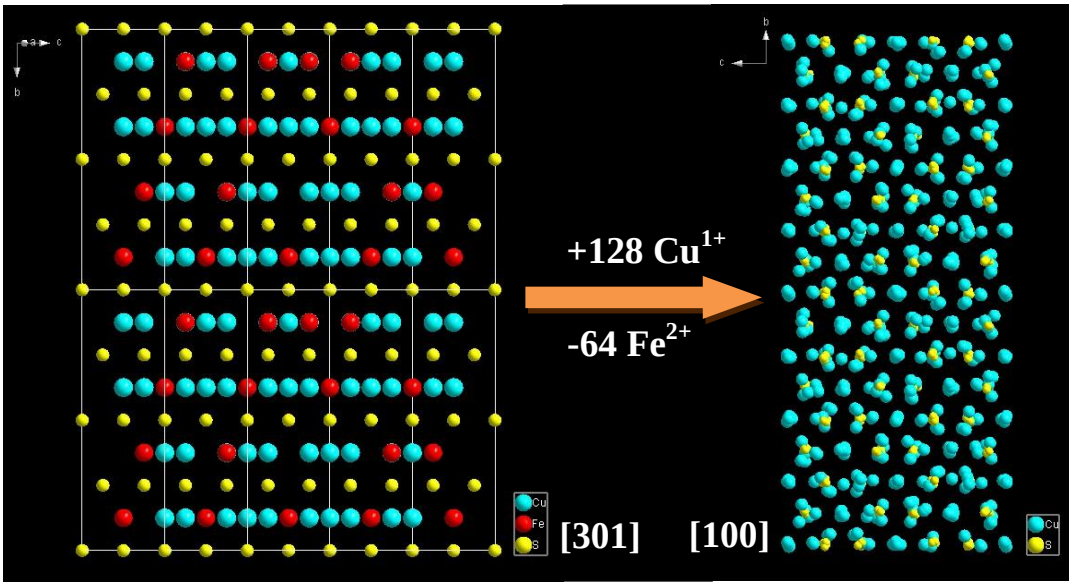

Figure S15: Four unit cells of Cu_5FeS_4 and corresponding conversion of one unit cell of $Cu_{1.97}S$.

XPS

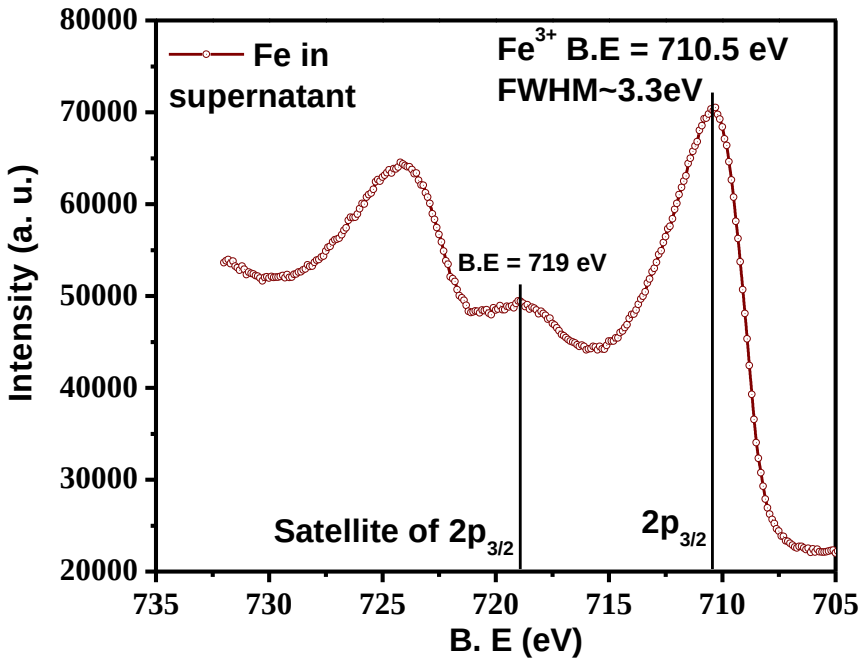

Figure S16. HRXPS spectra of supernatant after the cation exchange for the Fe_7S_8 to Fe_7S_8@Cu_5FeS_4 multigrain nanostructure. The FWHM of 2 P3/2 is 3.3eV and the presence of satellite of 2 P3/2 at binding energy 719 eV near the 2P1/2 peak concludes the supernatant mainly contained Fe in 3+ oxidation states[5].

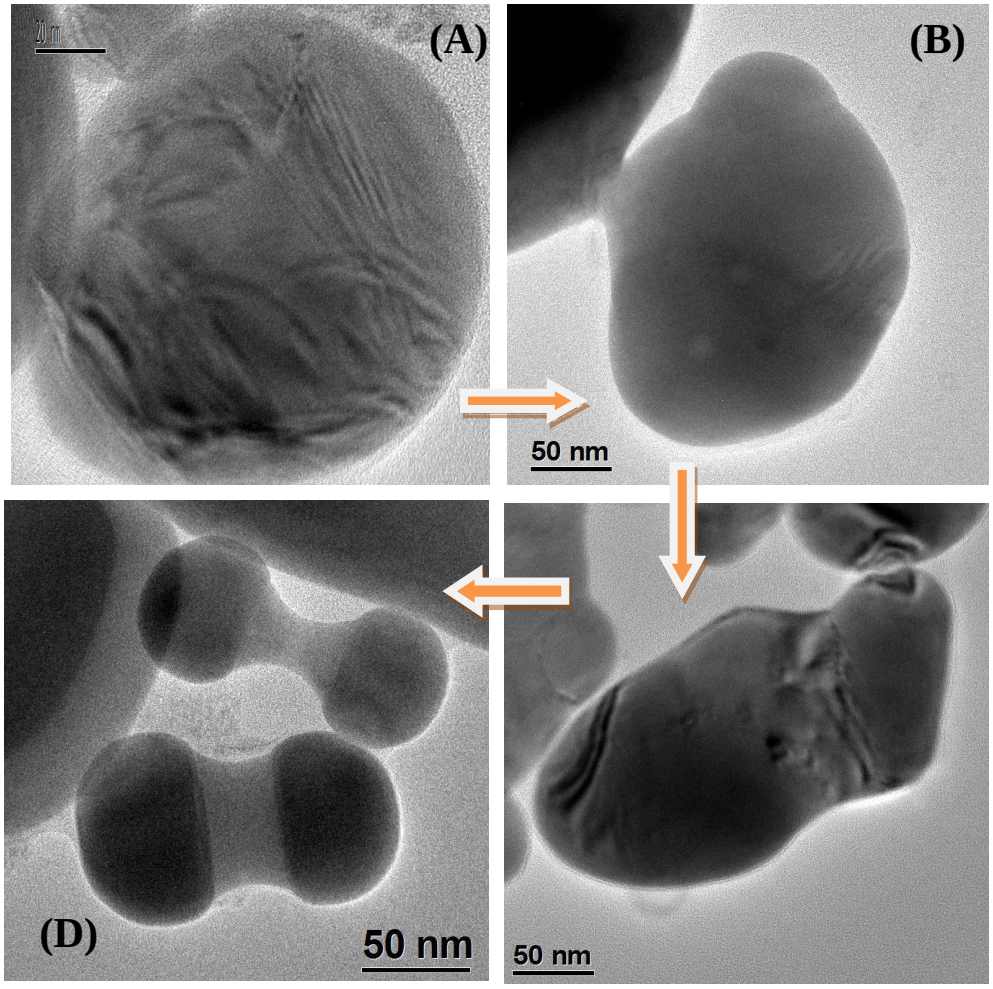

Figure S17. Time dependent conversion of Fe_7S_8 to $Cu_{1.97}S/Cu_5FeS_4/Cu_{1.97}S$ at Cu:Fe = 1.52. (A) 1 min, Multigrain structure, (B) 2 min, elongation of shape along opposite direction. (C) 3 min, Initiation of dumbbell formation. (D) 5 min, Nanodumbbell.

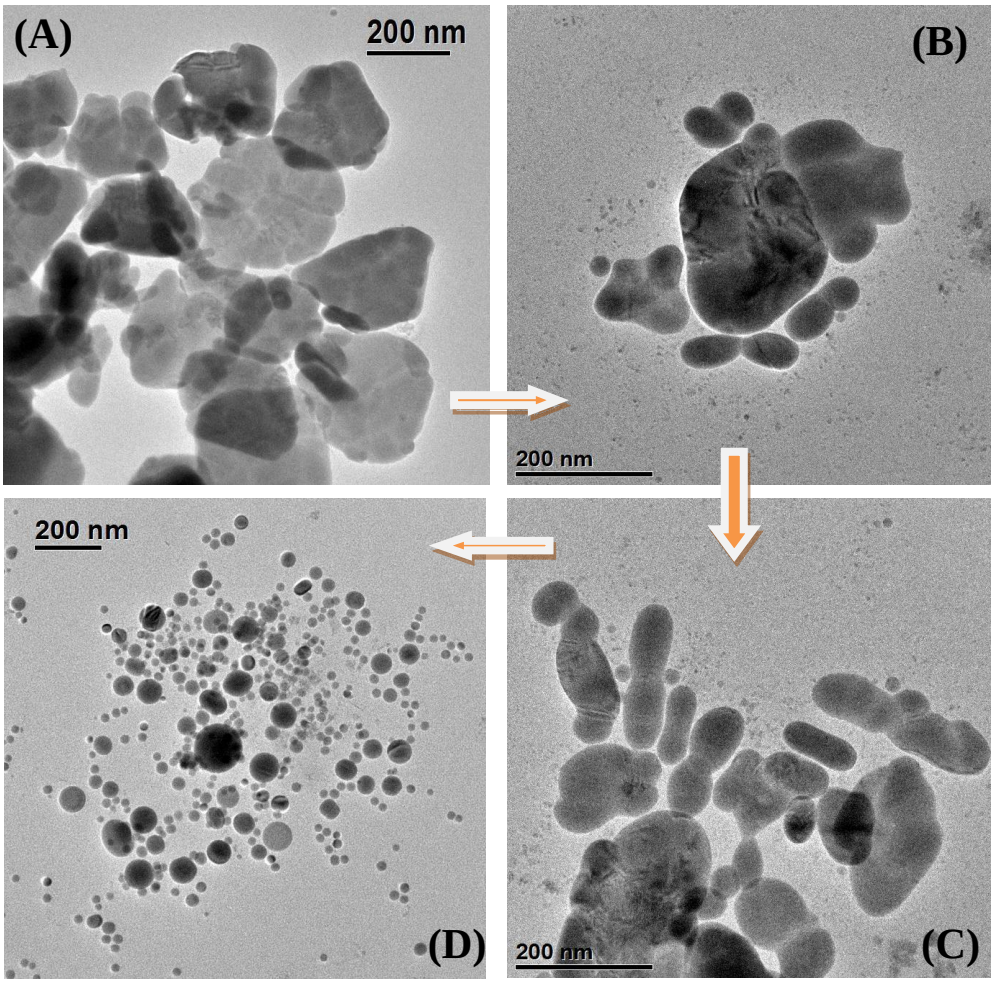

Figure S18: Time dependent conversion of Fe_7S_8 to $Cu_{1.97}S$ at Cu:Fe = 2.97. (A) 1 min, Multigrain structure, (B) 2 min, elongation of shape along opposite direction formation of nanodumbbell. (C) 3 min, nanodumbbells and formation of $Cu_{1.97}S$. (D) 5 min, Cu1.97S nanoplates.

ICP-AES

We have calculated the amount of Fe ejected for the conversion of Fe_7S_8 to Fe_7S_8/Cu_5FeS_4 core shell NHS and Fe_7S_8 to $Cu_{1.97}S/Cu_5FeS_4/Cu_{1.97}S$ nanodumbell by quantifying the amount of Fe present in wash liquid after separation of core-shell $Fe_7S_8@Cu_5FeS_4$ and $Cu_{1.97}S/Cu_5FeS_4/Cu_{1.97}S$ nanodumbell NHS by following previously reported protocol[6]:

Table S2: ICP-AES analysis.

Sample	Fe amount (mg/ml)		Ejected (Fe %)
	Before Cu addition	Final	
Fe_7S_8 to $Fe_7S_8@Cu_5FeS_4$	2.54	2.68	30.18%
Fe_7S_8 to $Cu_{1.97}S/Cu_5FeS_4/Cu_{1.97}S$	2.35	2.92	84%

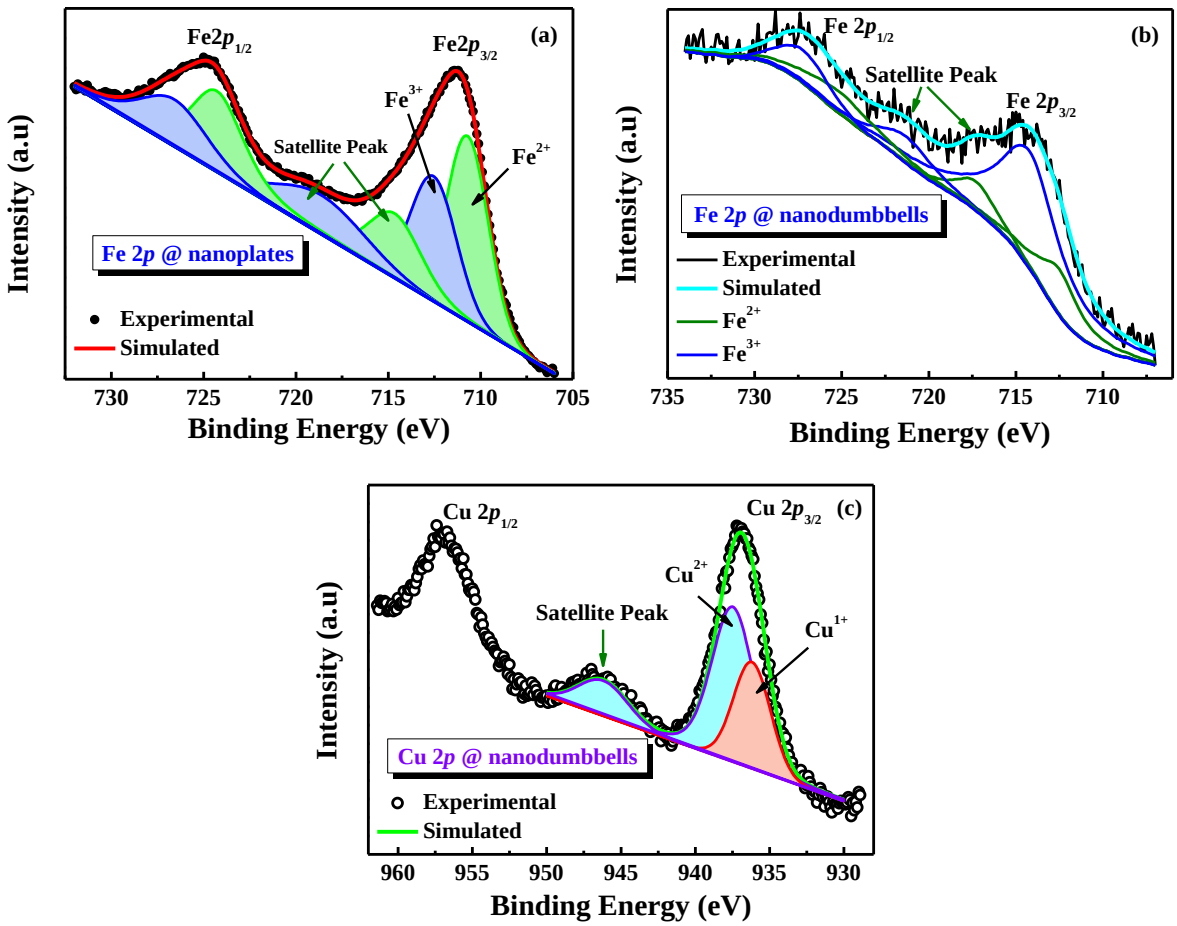

Figure S19. XPS analysis of Fe 2*p* core-level spectra represent the mixed valence state of Fe (Fe^{2+} and Fe^{3+}) in both (a) Fe_7S_8 nanoplates and (b) $Cu_{1.97}S/Cu_5FeS_4/Cu_{1.97}S$ nanodumbells. (c) Deconvulated XPS spectra of core-level Cu 2*p* in nanodumbell sample.

The ratio of Fe^{2+}/Fe^{3+}, obtained from the integrated intensity of the individual peak, is 1.32 for Fe_7S_8 nanoplates; in contrast to 2.5 for bulk Fe_7S_8. We can see that Cu 2p $_{3/2}$ can be resolved into two distinct peaks centered at 936.1 eV and 937.5 eV corresponding to the Cu^{1+} and Cu^{2+} states respectively. The satellite peak centered at 946.2 eV corresponds to the Cu^{2+} state. Thus XPS analysis depicts that Cu is in mixed valance state in nanodumbell sample although we have started the reaction with Cu^{1+} precursor. The presence of mix valancy of Cu suggests that Cu^{1+} oxidized to Cu^{2+} during reaction and increases the hole concentration of the sample which is responsible plasmonic absorption of the sample.

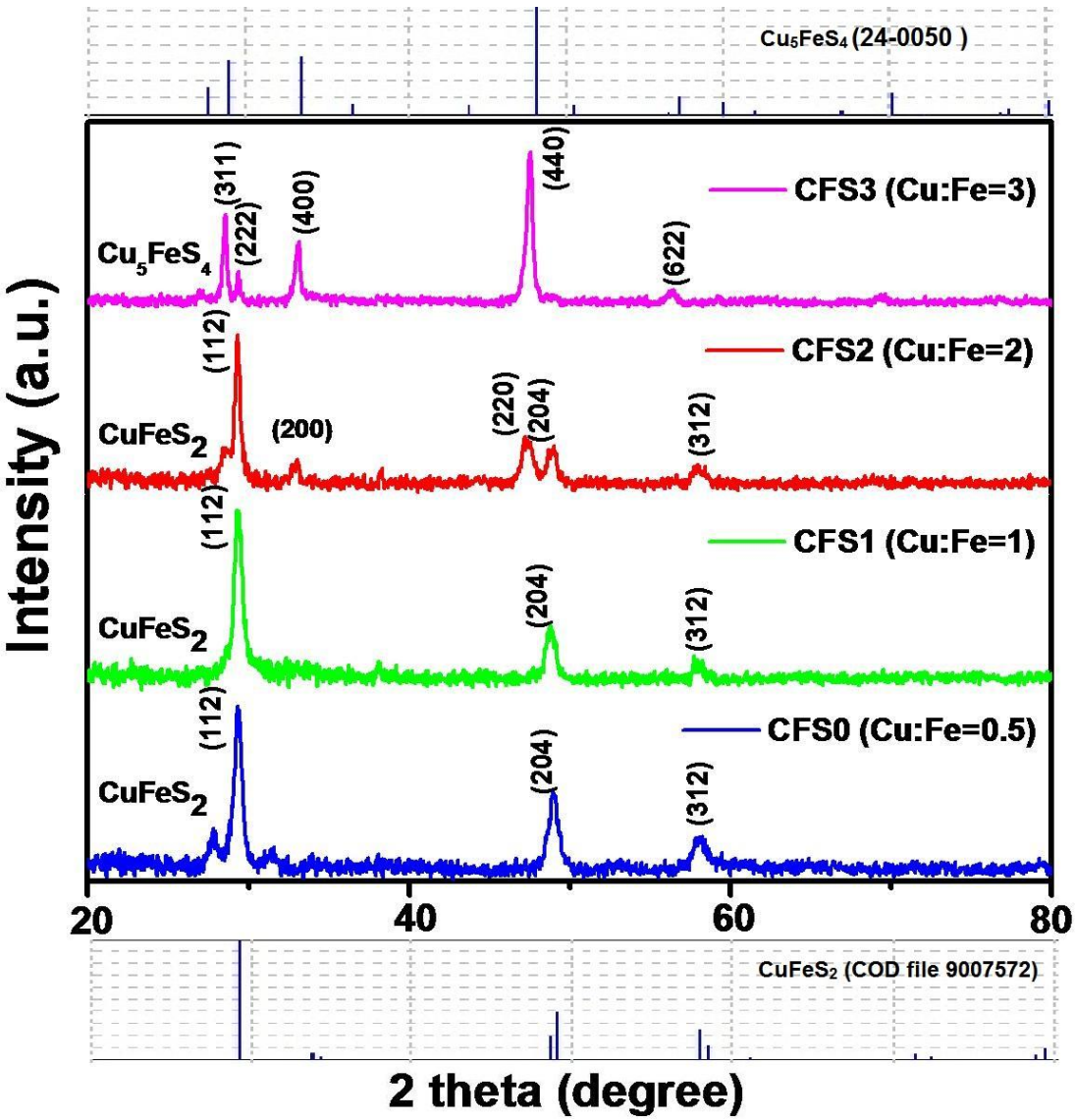

Figure S20. XRD pattern of different $CuFeS_2$ nanocrystals with variable amount of Cu: Fe.

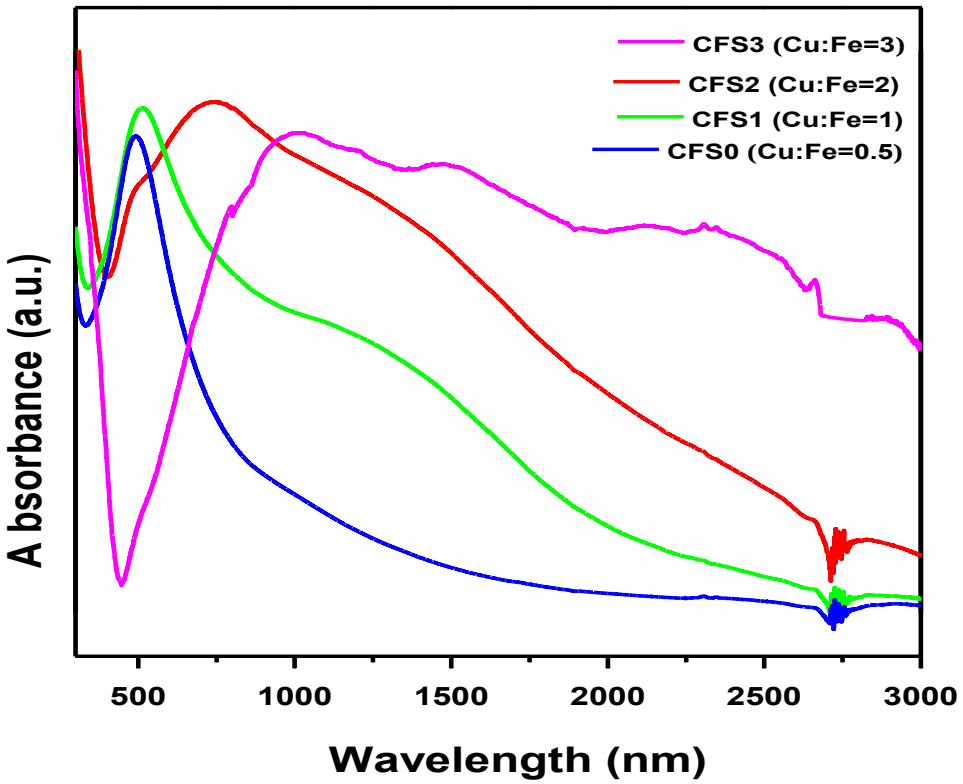

Figure S21. (A) Absorbance spectra of different $CuFeS_2$ nanocrystals.

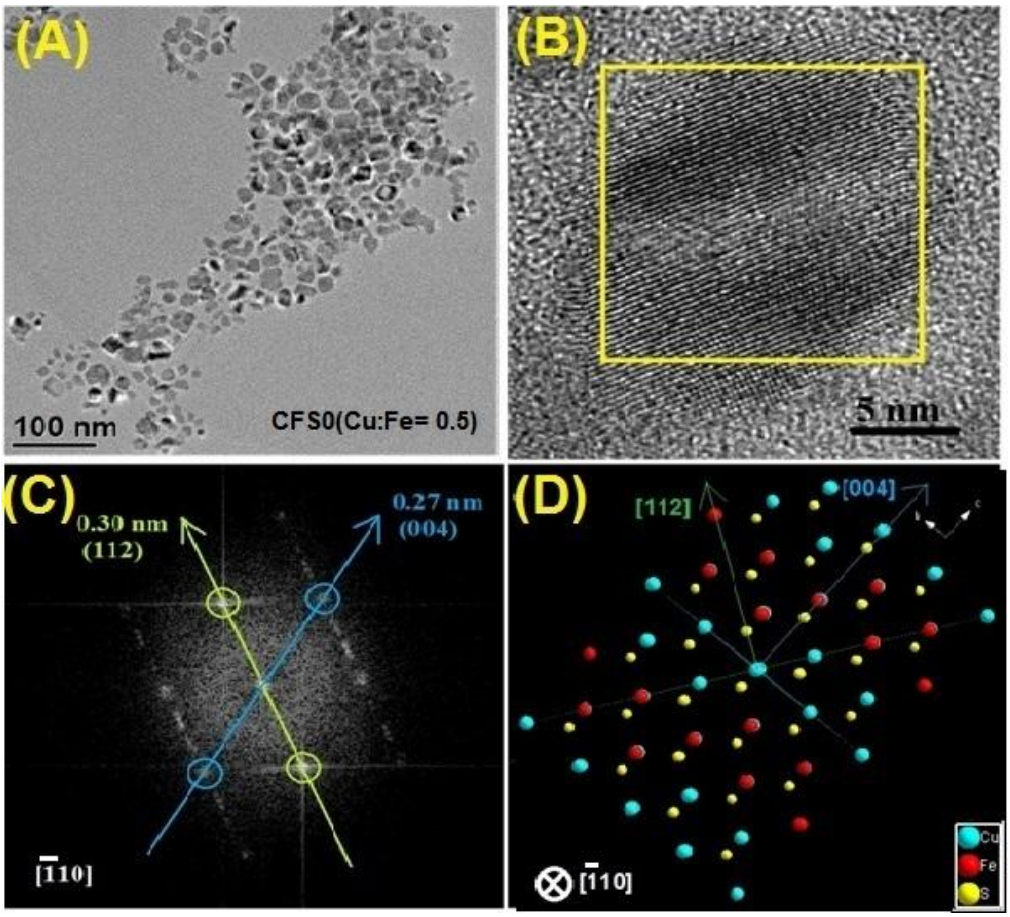

Figure S22. (A) Large area TEM image of CFS0 (Cu:Fe = 0.5). (B) HRTEM image and (C) corresponding FFT pattern. (D) Atomic model of Cu, Fe, S along the [-110] zone axis.

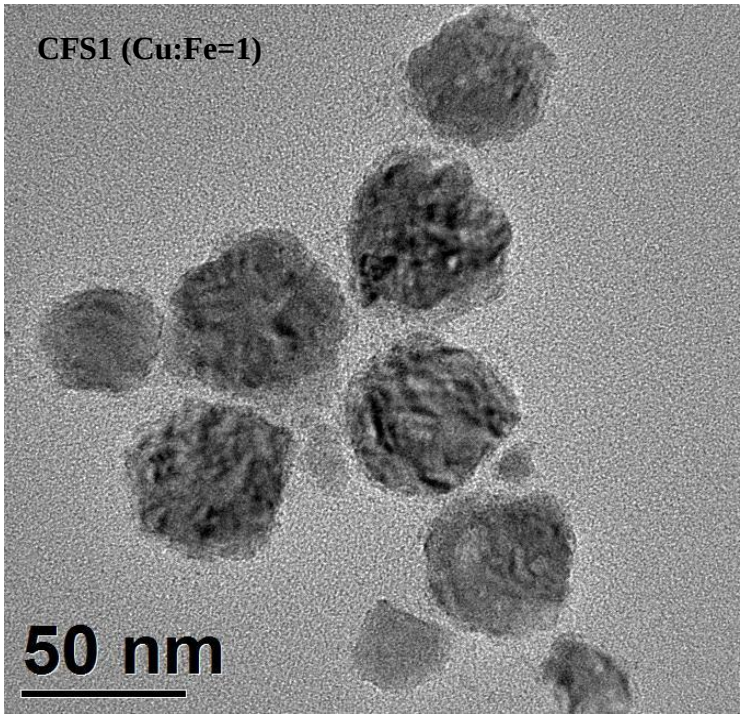

Figure S23.TEM image of CFS1 (Cu:Fe = 1).

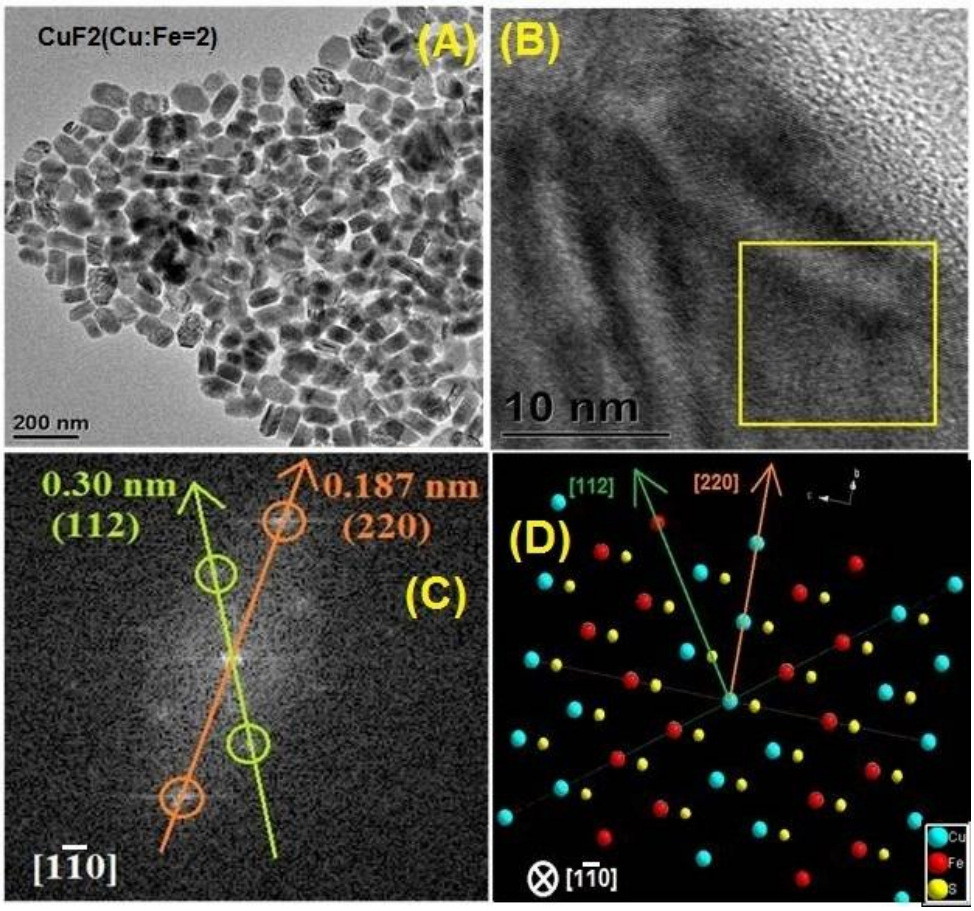

Figure S24. (A) Large area TEM image of CFS2 (Cu:Fe = 2). (B) HRTEM image and (C) corresponding FFT pattern. (D) Atomic model of Cu, Fe, S along the [1-10] zone axis.

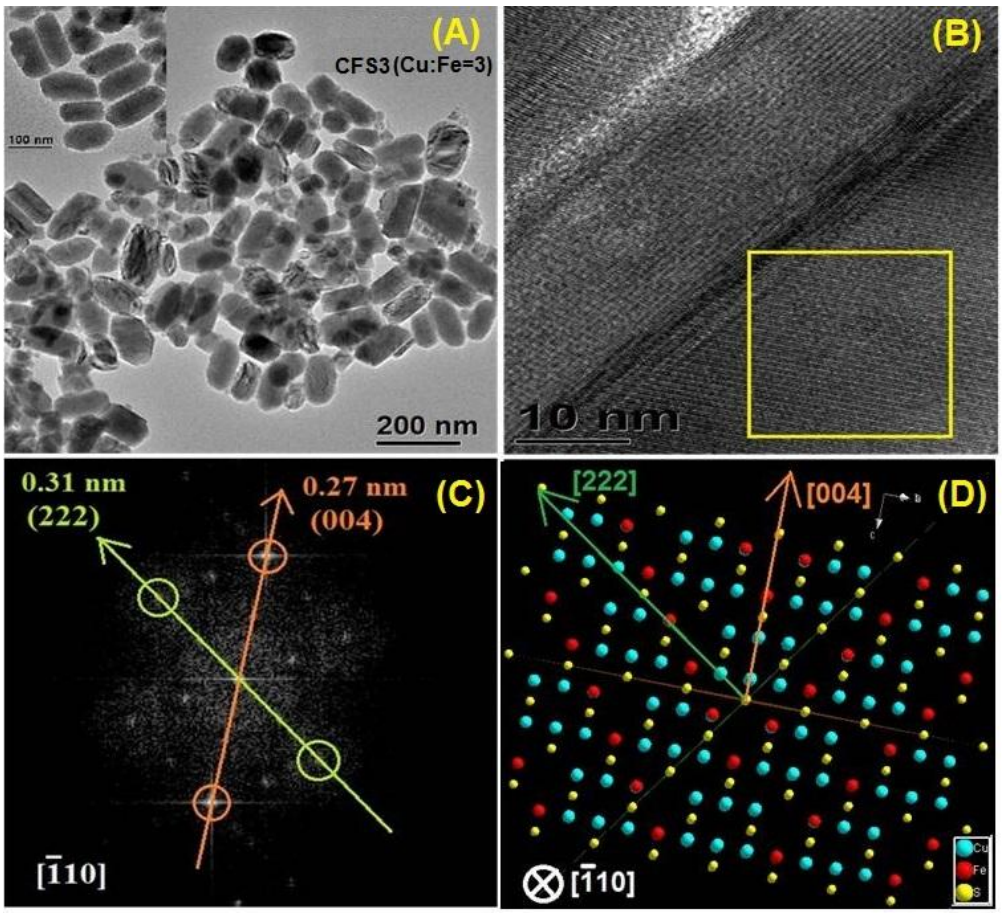

Figure S25. (A) Large area TEM image of CFS3 (Cu:Fe = 3). (B) HRTEM image and (C) corresponding FFT pattern. (D) Atomic model of Cu, Fe, S along the [-110] zone

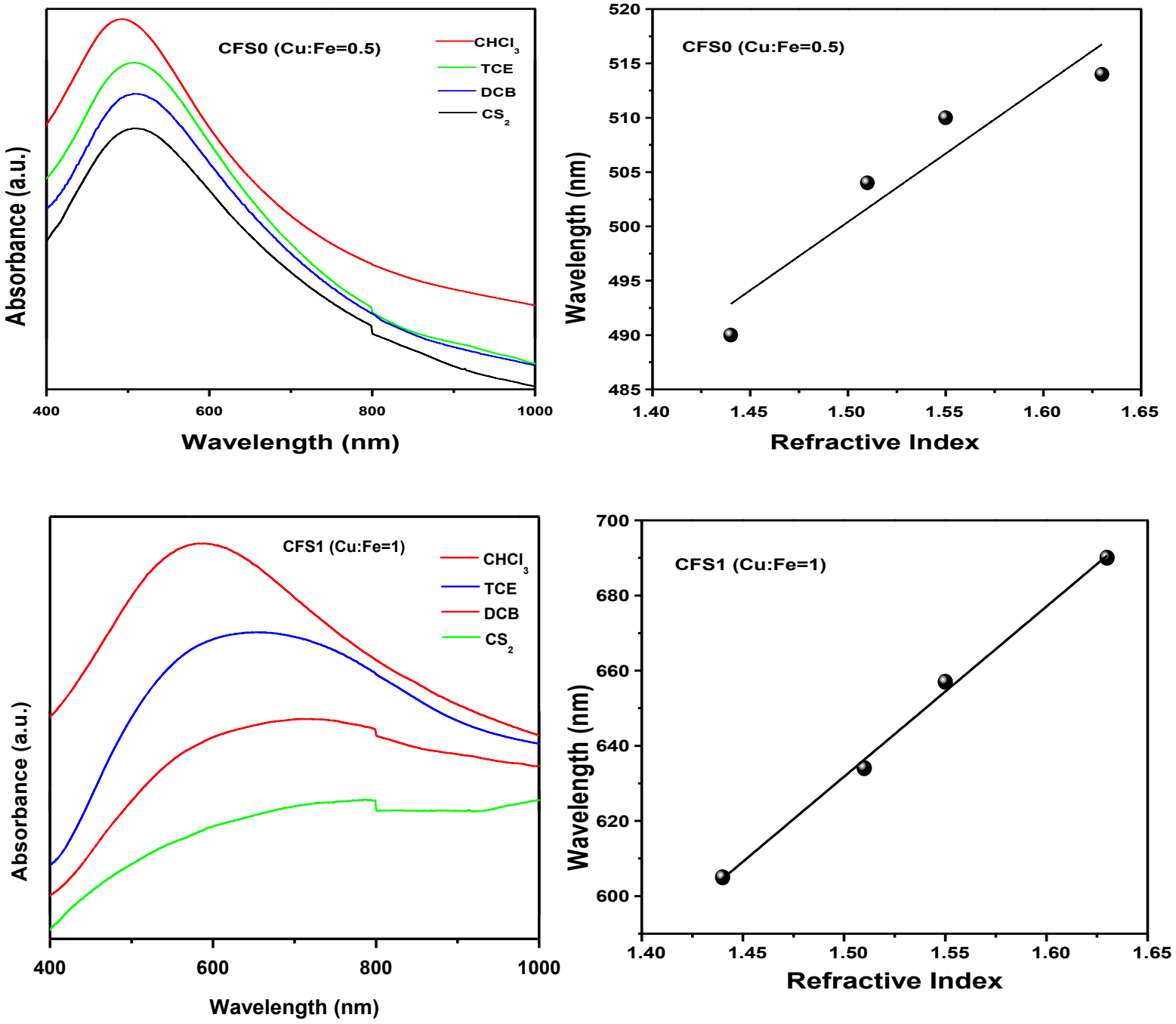

Figure S26. Solvent variation of absorption spectra and corresponding plasmonic sensitivity of samples CFS0 and CFS1.

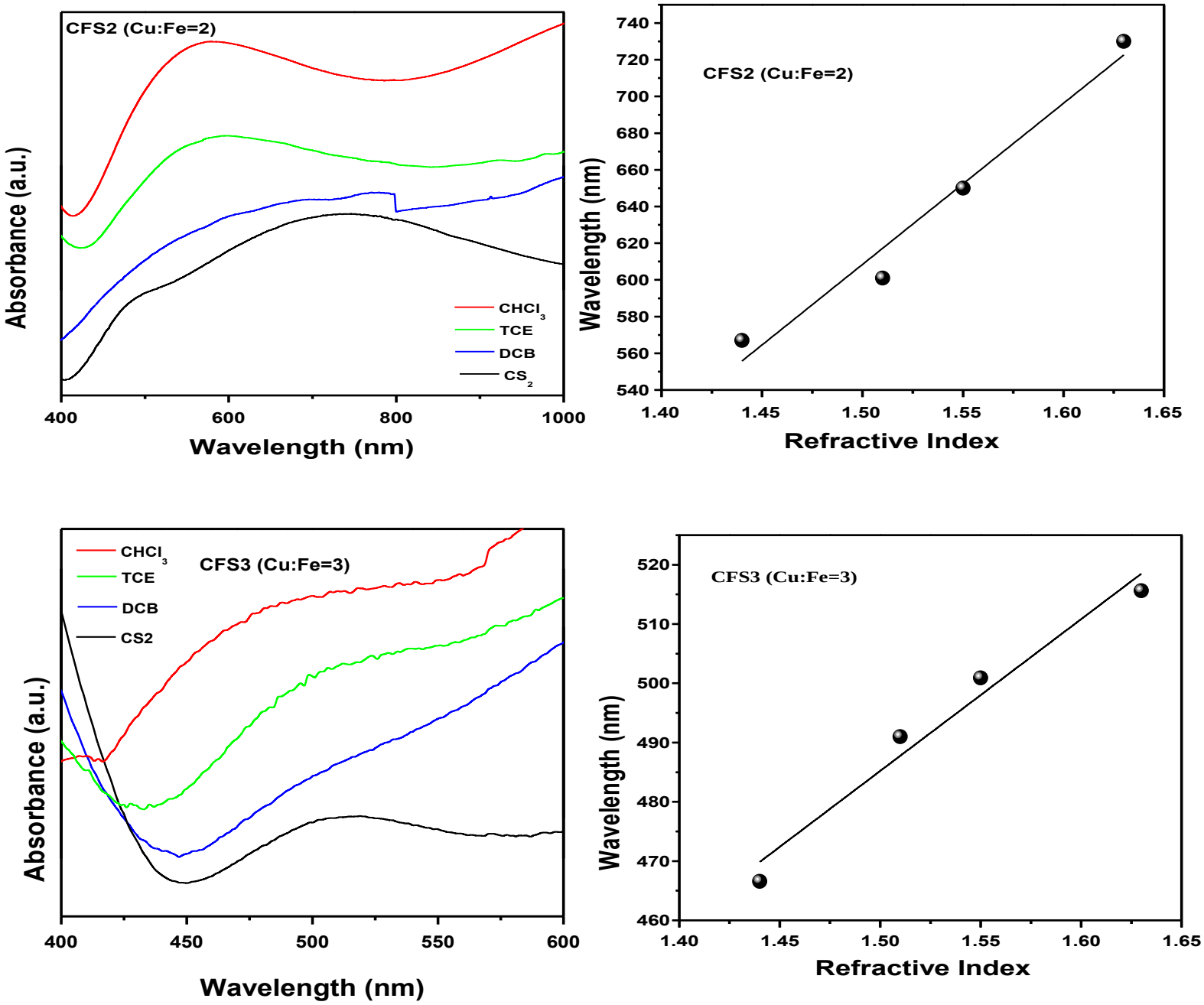

Figure S27. Solvent variation of absorption spectra and corresponding plasmonic sensitivity of samples CFS2 and CFS3.

Table S3: Summary of the morphology, plasmon peak position, plasmonic sensitivity of the samples (in-situ synthesis).

Sample (Cu:Fe precursor ratio)	Morphology /Dimension (nm)	Plasmon Peak Position (nm)	Plasmonic sensitivity (RI/nm)
CFS0	**Nanoparticle (15±3)**	**492**	**878.41**
CFS1	**Hexagonal (80±10)**	**452**	**452.72**
CFS2	**Nanodisks (100±10), (25±5)**	**850**	**125.82**
CFS3	**Nanocapsules (130± 25), (30±5)**	**1012**	**256**

References:

1. Ferrari, M. and Lutterotti, L. Method for the simultaneous determination of anisotropic residual stresses and texture by X-ray diffraction, *J. Appl. Phys.*, **1994**, *76* , 7246-7255.

2. Ding, Y.; Veblen, D. R. and Prewitt, C. T. Possible Fe/Cu ordering schemes in the 2*a* superstructure of bornite (Cu_5FeS_4), *Am. Mineral.*, **2005**, *90*, 1265–1269.

3. Evans Jr., H. T. Djurleite ($Cu_{1.94}S$) and Low Chalcocite (Cu_2S): New Crystal Structure Studies, *Science*, **1979**, *203*, 356-358.

4. Ding, X.; Bao, L.; Jiang, J. and Gu, H. Colloidal synthesis of ultrathin γ-Fe_2O_3 nanoplates, *RSC Adv.*, **2014**, *4*, 9314-9320.

5. Gota, S.; Guiot, E.; Henriot, M. and Gautier-Soyer, M. *Phys. Rev. B*, **1999**, *60*, 14387-14395.

6. Guria, A. K.; Prusty, G.; Chacrabarty, S. and Pradhan, N. Fixed Aspect Ratio Rod-to-Rod Conversion and Localized Surface Plasmon Resonance in Semiconducting I–V–VI Nanorods, *Adv. Mater.*, **2016**, *28*, 447–453.